JOURNAL OF SOLID STATE CHEMISTRY **128,** 197–204 (1997)
ARTICLE NO. SC967185

Band Electronic Structure Study of Some Doped and Undoped γ-Ln_2S_3 (Ln = La, Ce, Pr, and Nd) Rare Earth Sulfides through LMTO-TB Calculations

V. Zhukov,[1] R. Mauricot, P. Gressier,[2] and M. Evain

Laboratoire de Chimie des Solides, I.M.N., UMR CNRS N°110, Université de Nantes, BP32229, 2 rue de la Houssinière, 44322 Nantes Cedex 3, France

Received May 28, 1996; in revised form October 1, 1996; accepted October 14, 1996

The electronic structures of the γ-Ln_2S_3 (Ln = La, Ce, Pr, and Nd) light rare earth sulfides are studied by means of the *ab initio* self consistent LMTO-ASA method in the tight-binding representation. Results show that the valence and the conduction bands are mainly S 3*p* and *Ln* 5*d* in character, respectively, with the 4*f* levels in the electronic gap. A thorough analysis of the band energies and of the hybridizations leads to an interpretation of the compounds optical absorption edges, perfectly coherent with the experimental results. The influence of an alkali and alkaline earth metal insertion/substitution is discussed, and the effect on the band structure of a metal and/or sulfur nonstoichiometry is analyzed. © 1997 Academic Press

INTRODUCTION

In the search for new inorganic, nontoxic pigments, γ-Ln_2S_3 light rare earth sesquisulfides seem very promising (1). Possible colors are yellow, red, green, and light green for Ln = La, Ce, Pr, and Nd, respectively. A comparative study of these compounds, including the alkali and alkaline earth doped phases, was performed (2) with a view to identifying the transitions responsible for the colors. The study included structure determinations as well as electronic band structure calculations by means of the semi-empirical extended Hückel tight-binding method (EHTB). The main results are as follows: The γ-Ln_2S_3 structures derive from the Th_3P_4 structural type. In the cubic cell, each Ln rare earth atom sits in a triangular dodecahedral environment of 8 sulfur atoms. The rare earth atoms occupy 10.667 out of the 12 available sites per cell, thus the formulation $Ln_{2.667}S_4$ or Ln_2S_3. The vacant sites are randomly distributed throughout the structure. While the Ln_3S_4 phases are black metals, the γ-Ln_2S_3 phases exhibit semiconducting behavior. Surprisingly, the aforementioned color succession does not follow a straightforward, logical law. Apparently, the 4*f* orbitals seem crucial in the electronic absorptions responsible for the colors. When a γ-Ln_2S_3 phase is doped with an alkali or alkaline earth metal, A, a solid solution occurs. This solid solution results from a substitution/insertion of A (thereafter simply referred as doping) in the dodecahedral sites, preserving the charge neutrality (for instance, the limiting composition for Na doping is $Na_{0.5}Ln_{2.5}S_4$). Besides, spectroscopic studies show that localized levels are present within the band gaps of Ln_2S_3 compounds.

This paper reports a thorough analysis of the electronic structure of doped γ-$[A]Ln_2S_3$ and undoped γ-Ln_2S_3 rare earth sulfides (Ln = La, Ce, Pr, and Nd; A = Na) and of their Ln_3S_4 parent compounds. Section I presents a brief summary of the results previously obtained with the semi-empirical EHTB method (2) and some considerations on the limitations of the method. In Section II, new calculations by means of the self-consistent *ab initio* linear muffin-tin orbital method (LMTO) in the atomic spheres approximation (ASA) and in the tight-binding (TB) representation are then exposed. In Section III, the results are discussed: the origin of the γ-Ln_2S_3 colors and the effect of the doping are presented, and the influence of sulfur and metal vacancies on the band structure and on the optical properties is analyzed.

I. EHTB RESULTS FOR γ-Ce_2S_3

The band structure calculations performed by means of the EHTB method are fundamentally semi-empirical in nature (3). Moreover, they are realized in reciprocal space and thus, cannot take into account random vacancies. To model a lacunar structure, one can perform calculations for a stoichiometric compound, and then assume a rigid-band scheme to interpret the results. Such considerations are not too unrealistic if the densities of states (DOS) calculated for several lacunar structures, with arbitrary positions for the

[1] On leave from the Institute of Solid State Chemistry, Urals Branch of the Academy of Sciences, Pervomayskaya 91, 620219 Ekaterinburg, Russia.
[2] To whom correspondence should be addressed.

0022-4596/97 $25.00

vacancies, do not fundamentally depart from the DOS calculated for the pristine material. When dealing with rare earth elements, apart from the possible unreliability of the scarcely used H_{ii} parameters, the main limitation of the EHTB calculations is the absence of the 4*f* orbitals. One can exclude the 4*f* electrons from the valence electrons, but no real energy can be assigned to the 4*f* levels. Mauricot *et al.* recently reported (2) such EHTB calculations on γ-Ce_2S_3. In the following paragraphs, we summarize their major findings.

Figure 1 presents the band structure calculated with the EHTB method for Ce_3S_4, around the Fermi level and along the first Brillouin zone major symmetry lines shown in Fig. 2. The valence band (vb) (below -12.5 eV) is mainly S 3*p* in character, while the conduction band (cb) (above -10.5 eV) is chiefly Ce 5*d*. The Fermi level (straight line) intersects wide bands in all directions, in agreement with the isotropic metallic behavior of Ce_3S_4. Within a rigid-band scheme, a stoichiometry alteration from Ce_3S_4 to $Ce_{2.667}S_4$ results in the total emptying of the cb. A Mulliken population analysis indicates that this depletion strengthens the bonding character of the Ce–S bond. It also shows that weak bonding interactions exist between the cerium nearest neighbors ($d_{Ce-Ce} = 4.034$ Å).

As can be seen in Fig. 1, the gap for Ce_2S_3 is indirect, from the bottom of the cb at Γ to the top of the vb at a point between Γ and H. This observation is confirmed by ellipsometry studies which show an indirect gap of 2.75 eV (4). The energy gap is usually largely overestimated in EHTB calculations but, since it is strongly dependent on the H_{ii} parameters, it can easily be adjusted. This is the case in the reported calculations where the Ce 5*d* energy state has been arbitrarily lowered. The results nevertheless clearly indicate that the energy gap should not be fundamentally modified when going from La to Gd, along the lanthanide series.

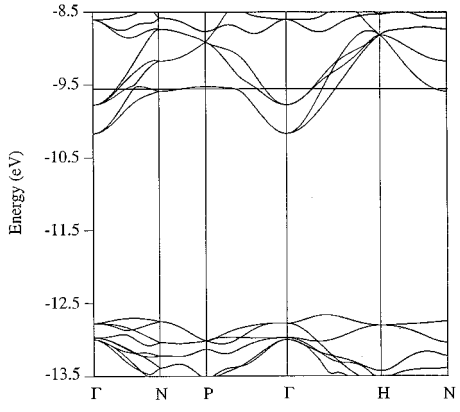

FIG. 1. EHTB band structure near the Fermi level of Ce_3S_4. The Brillouin zone special points Γ, H, P, and N are defined in Fig. 2.

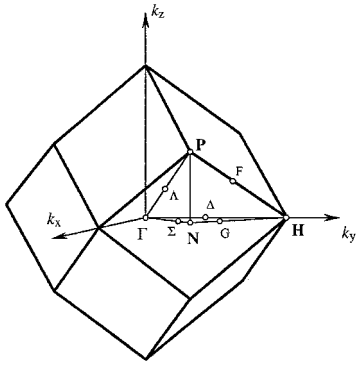

FIG. 2. First Brillouin zone of $Ce_{12}S_{16}$ body-centered cubic cell.

From the 4*f* energy levels deduced by Kaciulis *et al.* from XPS studies (5), an absorption mechanism is proposed for the γ-Ln_2S_3 phases (Ln = La, Ce, ... , Gd). For lanthanum, a vb → cb absorption takes place with an energy gap leading to the yellow color of γ-La_2S_3. For the following rare earth elements, the XPS results indicate that the 4*f* energy band is above the vb for γ-Ce_2S_3, but then progressively drops when the atomic number Z increases. The Ce_2S_3 red color is thus attributed to a $4f \rightarrow$ cb transition. For neodymium, the 4*f* level would be close to the top of the vb, leading to a vb → cb transition and therefore a greenish-yellow color. For the next elements of the rare earth series, the various possible transitions between the 4*f* terms should be considered.

Since the alkali and alkaline earth metals are poorly modeled by the EHTB method, they were not introduced in the calculations. Simple considerations led the authors to conclude that the doping should stabilize the overall structure by filling the empty sites without altering the charge neutrality. EHTB calculations are irrelevant in that respect.

The XPS spectra reported in Ref. (5) have a low resolution. In addition, they do not directly give the energy positions of the bands because they incorporate relaxation terms intrinsic of the photoemission process. Since the localization of the 4*f* levels is crucial for the interpretation of the γ-Ln_2S_3 colors and since the understanding of the doping process is important for possible color modifications, new calculations by means of the self-consistent *ab initio* LMTO-ASA method in the TB representation were initiated.

II. LMTO-ASA CALCULATIONS

II.1. Presentation and Limitations of the Method

Among the nonempirical methods for band structure calculations, the most successful are based upon the density functional theory (DFT) in its local spin density approximation (LSDA) (6). These methods do not consider individual electrons, but the whole many-body electron system through the total electron density $\rho(\mathbf{r})$. The total energy E,

which is written as a functional of $\rho(\mathbf{r})$, can be split as a sum of three terms

$$E[\rho] = T[\rho] + V[\rho] + E_{xc}[\rho],$$

where $T[\rho]$, $V[\rho]$, and $E_{xc}[\rho]$ are the kinetic, potential, and exchange-correlation energies, respectively. In the LMTO-ASA method (7), the shape of the crystal potential is simplified in the form of a spherical, symmetric potential around the atoms (then including both the nuclei and the core electrons) and a constant potential between the atomic spheres.

Although successful in most cases, LSDA-based methods should be cautiously considered when dealing with 4*f* orbitals. Indeed, in these methods the exchange-correlation potentials are usually derived from various theories on exchange and correlation in a homogeneous electron gas. Since the 4*f* orbitals are highly localized, the LSDA-based methods may not be adequate for their study. It was recently shown (8) that the spin correlations are generally treated with sufficient precision but that the Coulomb correlations in 4*f* and heavy-*d* electron systems are described with great errors. A number of corrections have been proposed for fixing these problems. Among them is the use of on-site Coulomb repulsion parameters and in some cases of nondiagonal Coulomb and exchange corrections (8, 9). In fact, the introduction of a Coulomb on-site repulsion parameter, *U*, is very important in the case of compounds with 4*f* orbital elements (a typical *U* value for 4*f* orbitals is ca. 6–9 eV). Without these corrections the position of the 4*f* bands is presumably inaccurate, which in turn corrupts the energy of the bands that are strongly hybridized with those 4*f* orbitals (10). Fortunately, among the rare earth elements with 4*f* electrons, cerium is certainly the element the less prone to yield large errors since it has only one 4*f* electron and the less localized 4*f* orbitals. Moreover, the Ce–Ce distance in γ-Ce_2S_3 (4.034 Å) is rather large compared to the distance found in γ-Ce (3.65 Å) where the 4*f* orbitals hardly interact (10). However, the position of the 4*f* bands is a result of a balance between the positive Coulomb correlation energy and negative exchange energy, those terms being the largest for the *f* orbitals among all types of atomic orbitals. Therefore, the position of the 4*f* states is very sensitive to the details of the calculations, for instance the shape of the 4*f* orbitals which can themselves bear errors due to the inaccuracy of the Coulomb correlations.

The second problem that could arise is directly related to the particular aim of our study, the determination of optical gaps. Indeed, in the LSDA-based methods, any valence electron interacts with itself by means of the Coulomb potential. This may not be of great importance in the case of elementary solids, since the self-interaction (SI) only shifts the valence states uniformly along the energy scale; but it can introduce errors in determining the band gap between the *Ln* 5*d*-like cb and the S *p*-like vb, since the cb and the vb have different space shapes and consequently different SI errors. A number of methods to calculate SI corrections have been proposed (11). Generally these methods use the different *k*- and band-dependent SI corrected potentials, so that their incorporation in computer codes is difficult. Up to now, such studies have been limited almost exclusively to pure metals (12).

The determination of the ground state of the electronic structure of the γ-Ln_2S_3 phases with a LSDA-based method seems to be a difficult task, and the characterization and quantification of the band gap (which is related to excited states and thus should take into account various electronic configurations) go beyond the LSDA approximation. Nevertheless, keeping in mind the various drawbacks of the method, calculations were carried out on the $Ln_{3-x}S_4$ series in order to evaluate the evolution of the optical properties as a function of *Z*, as a function of doping, and as a function of vacancy content.

II.2. Computational Details

The LMTO-ASA method is especially well adapted to the study of compact structures where the Wigner–Seitz spheres almost completely fill the space. This is the case for the Th_3P_4 structure type. In open or lacunar structures, empty interstitial spheres have to be introduced to prevent large overlaps, misrepresentations of the potential, and lacks of charge densities. In the calculations for the Ln_2S_3 compounds (atomic positions of the rare earth and sulfur atoms taken from Ref. (2)), one rare earth atom out of six was replaced by an empty sphere (*E*) to reach the Ln_5ES_8 ($Ln_{1.875}S_3$) atomic composition (close to the original Ln_2S_3 stoichiometry and to be referred as Ln_2S_3 thereafter). Such a setting explicitly excludes the observed disorder associated with the cation random distribution over the dodecahedral sites.

The calculations were performed by using the tight-binding representation of the LMTO-ASA method (13a). The Wigner–Seitz's atomic sphere radii (see Table 1) have been determined by using the automatic procedure reported in Ref. (10). The usual LMTO-ASA criterion of totally filling

TABLE 1
Atomic Spheres Radii (Å) Used in the LMTO-ASA Calculations

Compound	*r*(*Ln*, *E*)	*r*(S)
La_3S_4	2.00	1.58
La_2S_3	2.02	1.56
Ce_3S_4	1.92	1.63
Ce_2S_3	2.00	1.54
Pr_2S_3	1.98	1.52
Nd_2S_3	1.97	1.52

the crystal volume by the atomic spheres was used, together with the combined correction (13b). The sphere radii are chosen under the requirement that the superposition of the spherical potentials be the best possible approximation to the full potential. As the combined correction introduces a kinetic-energy error proportional to the 4th power of the relative sphere overlap, the usual condition to get accurate calculations is that the radial overlap for any couple of spheres should be no more than 15% of the distance between the centers of the given spheres. This condition is satisfied in the present case by using empty site spheres. The atomic partial waves used in the calculations were 6*s*, 6*p*, 5*d*, and 4*f* for *Ln* atoms, 3*s*, 3*p*, and 3*d* for sulfur atoms, and 1*s*, 2*p*, and 3*d* for the vacancies. However, the 6*p* *Ln* states, 3*d* S states, and 2*s* and 3*p* vacancy states were not directly included in the basis set but "down-folded" using the Lowdin's perturbation technique incorporated in the TB LMTO-ASA codes (13c). The *k*-space integrations were performed with the tetrahedron method (14). The numbers of *k*-vectors per irreducible wedge of the Brillouin zone used in the various calculations were 134 for the La compounds and 1034 for the Ce, Pr, and Nd compounds, which was sufficient to get a slow, smooth convergence of the self-consistency processes.

Spin-polarized calculations of the electronic band structure have also been performed for Ce_2S_3. The essential change with respect to the results without a spin-polarization was a shift of the 4*f* minority spin states of 0.8 eV to higher energies; no noticeable changes in the $4f \leftrightarrow$ cb and vb $\leftrightarrow$ cb energy gaps were observed. Therefore such calculations have been omitted for the other compounds.

III. RESULTS AND DISCUSSION

III.1. Density of States (DOS)

The calculations show, as for the EHTB calculations, that the vb is mainly built up from the S 3*p* states in bonding interaction with the *Ln* 5*d* states, while the cb is essentially made up of the *Ln* 5*d* antibonding crystal orbitals. The total DOS of La_3S_4, Ce_3S_4, γ-La_2S_3, and γ-Ce_2S_3 are shown in Fig. 3. If one excludes for obvious reasons the La compounds, it can be seen that the sharp 4*f* band is located within the vb $\leftrightarrow$ cb band gap. The Fermi level is therefore located within the 4*f* band. This is incompatible with the metallic and optical properties of the Ln_3S_4 phases. So we have a good example of the breakdown of an LSDA-based method. Nevertheless the calculations provide rational clues toward the understanding of the electronic structure of the intermediate, $x > 0$, $Ln_{3-x}S_4$ sulfides. For γ-Ce_2S_3, i.e., the lower limit of the $Ce_{3-x}S_4$ series, the S 3*p*-like vb is completely filled and the Ce 5*d*-like cb is empty, while the Ce 4*f* band contains one electron per Ce atom. For $x < 1/3$, i.e., for higher Ce content, the additional electrons cannot occupy the empty levels of the 4*f* one-electron band because of strong coulomb correlations. They could occupy the upper Hubbard band, but it would be ca. 6 eV above the lower 4*f* Hubbard band, that is, well above the 5*d*-like states. Therefore, they occupy the 5*d* states and are localized by an Anderson's mechanism due to the rare earth sublattice disorder. Such a mechanism leads to a hopping conductivity for the $Ln_{3-x}S_4$ compounds, as reported in Ref. (16).

III.2. Gaps and Optical Properties

The establishment of reliable relations between the optical properties and the electronic structures of the rare earth sesquisulfides has for a long time been the quest of many research groups (17–19). The present study adds some qualitative and quantitative aspects to that aim. The most relevant result is the quantification of the vb or 4*f* band $\leftrightarrow$ cb energy gaps, as plotted in Fig. 4. It follows from our results that the fundamental absorption onset for γ-La_2S_3 is provided by S $3p \leftrightarrow$ La 5*d* (vb $\leftrightarrow$ cb) excitations, while it comes from 4*f* to 5*d* transitions for *Ln* = Ce, Pr, Nd. A noticeable increase of the vb $\leftrightarrow$ cb gap takes place between La and Ce. Then, between Ce, Pr, and Nd, the gap value changes smoothly. The $4f \leftrightarrow$ cb energy gap increase for the heavier elements is related to the usual decrease of the 4*f* state energies in the rare earth series. This is in agreement with the XPS results (5). In γ-Pr_2S_3 and γ-Nd_2S_3, the 4*f* states are near the top of the vb, in coherence with magneto-optic effect studies by Babonas *et al.* (18) and reflection measurements by Zhuze *et al.* (19).

Due to the small difference between the vb $\leftrightarrow$ cb gaps and the experimental gaps found for the praseodymium and neodymium compounds, it is not clear which values, the vb $\leftrightarrow$ cb or the $4f \leftrightarrow$ cb energy gaps, should be compared to the experimental values. However, the trend in the variation of the calculated $4f \leftrightarrow$ cb gaps reproduces quite well the variation in the series of experimental gaps. The conclusion is that in this series of compounds the 4*f* states seems to take part in the chemical bonding, hybridizing with the 3*p* sulfur states and pushing the valence band states to lower energy.

Figure 5 presents the band structure of La_3S_4 calculated with the TB LMTO-ASA method, around the Fermi level and along the symmetry lines used in Fig. 1. It is worth noticing that the band structure aspect is very similar to that calculated with the EHTB approach for Ce_3S_4. The indirect character of the band gap, between Γ and H, is confirmed.

III.3. Sodium Doping

To model the sodium doping (insertion/substitution) the calculations were performed on an unit cell of composition Ln_5NaS_8 (*Ln* = La and Ce). The formula Ln_5NaS_8 ($Ln_{2.5}Na_{0.5}S_4 = Ln_{1.875}Na_{0.375}S_3$) actually corresponds to

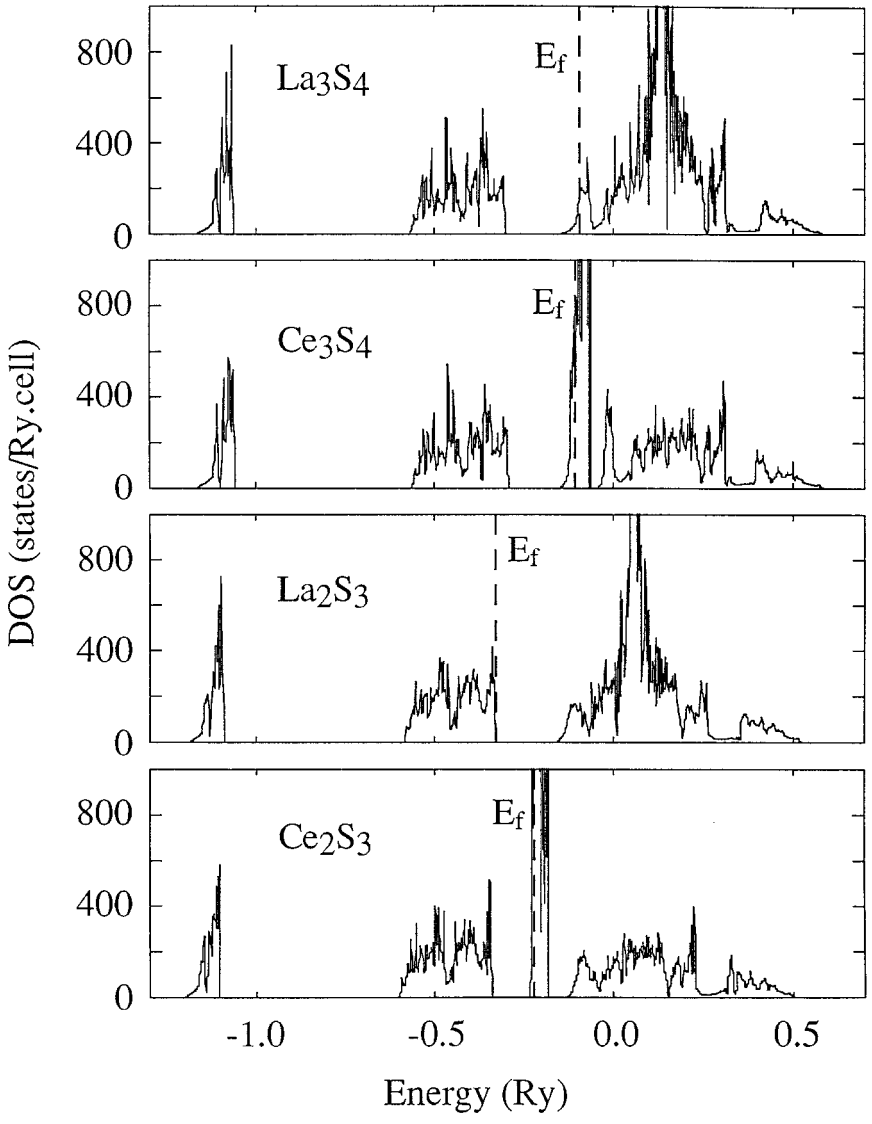

FIG. 3. DOS of La_3S_4, Ce_3S_4, La_2S_3, Ce_2S_3. (states per Ry per $Ln_{12}S_{16}$ or $Ln_{10}S_{16}$ unit cell).

the upper limit of the sodium content (2) and disregards the statistical distribution. Due to their high energy, the 3*s*, *p* Na states do not markedly change the band structures. However, various modifications can be noticed. Since there is an effective charge transfer from the sodium atoms to the cerium and sulfur spheres, the Coulomb correlation energies of the Ce and S states increase. The more localized the orbital, the larger the increase: the energy center of gravity of the band is raised by ca. 0.17, 0.35, and 0.42 eV for the sulfur *s* and cerium *d* and *f* states, respectively. Based upon this sole consideration, the optical gap is predicted to increase for γ-[Na]La_2S_3 (vb$\leftrightarrow$cb gap) but decrease for γ-[Na]Ce_2S_3 ($4f\leftrightarrow$cb gap). However, since the sulfur *p*–cerium *f*, *d* state separation increases, the interaction is reduced and so are the band widths (it is worth mentioning that the hybridization of the cerium *f* states with the sulfur *p* states, although very small, is about the same as that between the cerium *f* and *d* states). This last effect prevails for γ-[Na]Ce_2S_3 and leads to a slight global increase of the $4f$–cb gap (ca. 0.2 eV), which is close to the experimental findings of Mauricot *et al.* (2).

Chemically speaking, the sodium insertion/substitution process increases the overall ionicity of the structure. This leads for γ-Ce_2S_3 to a change of the material color from maroon to red-orange, though a profound modification of the γ-Ln_2S_3 initial color cannot be achieved in this way because of the small changes in the density of states. However, since the optical gap depends directly on the

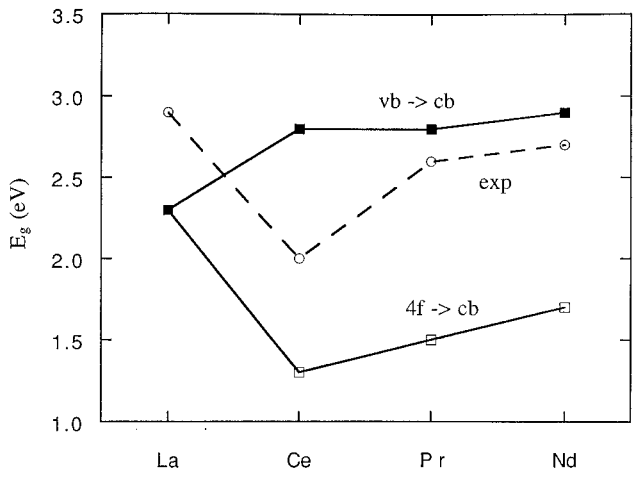

FIG. 4. Energy gaps as a function of the atomic number. See text for explanation.

nature of the fundamental absorption edge, deeper color changes could be realized through a partial substitution of the cerium atom by other rare earth elements.

III.4. Sulfur and Metal Vacancies

When performing precise optical analyses, one usually faces a more intricate band picture than the diagram given by band structure calculations. For instance, the photoconductivity spectra of γ-La_2S_3 (20), γ-Ce_2S_3 (21), γ-Nd_2S_3, γ-Gd_2S_3 (2b), and γ-Dy_2S_3 (22) all exhibit common peaks at lower energy than the vb↔cb transition, probing so-called impurity or localized states in the band gap. Through thermally stimulated current experiments, Georgiobani *et al.* (20) observed photoconductivity trap levels in γ-La_2S_3, localized below cb. Using time-resolved fluorescence, Mauricot *et al.* (23) observed slow decay fluorescence from an emitting level localized below cb for γ-La_2S_3 and γ-Ce_2S_3. Except for La, 4*f* orbitals may provide levels near the top of vb, but, as already shown, their positions shift with *Z*. However, a common feature of these compounds is the occurrence of intrinsic metal vacancies and the possibility of sulfur vacancies. In this section it is shown that the metal and sulfur vacancies can give rise to localized states near the top of vb and the bottom of cb, respectively.

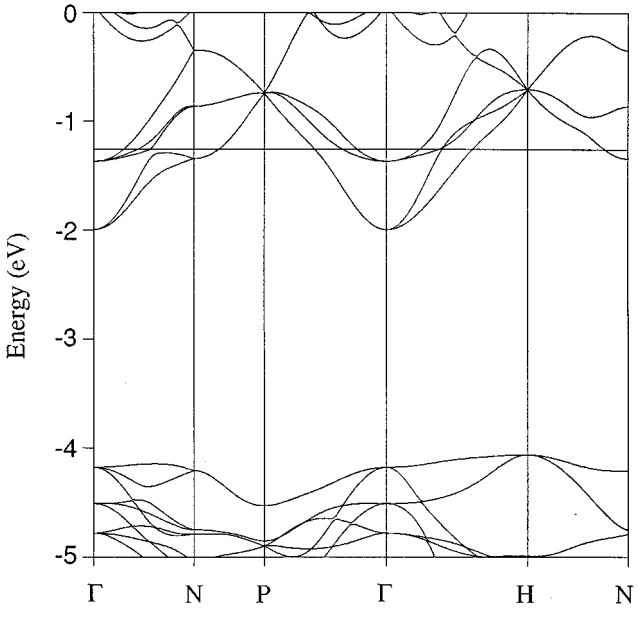

FIG. 5. Dispersion curves along the main directions of the Brillouin zone for La_3S_4.

To model the nonstoichiometry of the sulfur sublattice, one sulfur atom of the extended γ-La_3S_4 structure has been replaced by an empty sphere with an *s* orbital basis and down-folded *p* and *d* orbitals, keeping the sphere radii unchanged. This lacunar structure will be thereafter referred to as $La_{12}S_{15}$. We also performed calculations using a unit cell made up of five metal atoms, one vacancy in the metal sublattice, seven sulfur atoms, and one vacancy in the sulfur sublattice, i.e., an La_5S_7 composition.

In Fig. 6 the DOS for $La_{12}S_{15}$ and the relative projected density of states per atom, PDOS/DOS, of the sulfur vacancies are reported. The PDOS/DOS curve, which gives the integrated (over the Brillouin zone) orbital characters of the given atom (vacancy) as a function of energy, is less cumbersome than the usual more instructive "fat band" curves, which give the orbital character weighted band structure. Figure 7 presents similar curves (DOS and PDOS/DOS of the lanthanum vacancy) calculated for La_5S_7 in the lower energy region.

The signature of localized states due to the presence of vacant sites in metal and nonmetal sublattices in band structure calculation has already been discussed in various publications (24, 25). In Ref. (24) the effect of periodic vacancies in nonstoichiometric titanium oxide TiO_{1-x} ($x = 0.25$) was analyzed by the Augmented Plane Wave (APW) method. In Ref. (25) similar effects were looked for in transition metal carbides MC_{1-x}, (M = Ti, Zr, Hf; x ranging from 0 to 0.4) with the KKR–CPA (Korringa Kohn Rostoker–Coherent Phase Approximation) method. In this last study it was found that for small x values a narrow peak emerges in the density of states near the cb and that the larger the x content, the wider the separation of this peak from cb. Besides, when x approaches 0.2, a splitting of the vacancy peak occurs, which is also observed in the APW calculations. The qualitative interpretation for the vacancy state formation is as follows. The removal of a nonmetal atom from the lattice results in a breakdown of the nearest-neighbors metal–ligand hybridization. This induces a decrease in energy of the electronic state initially in cb because it was antibonding with respect to the metal–ligand

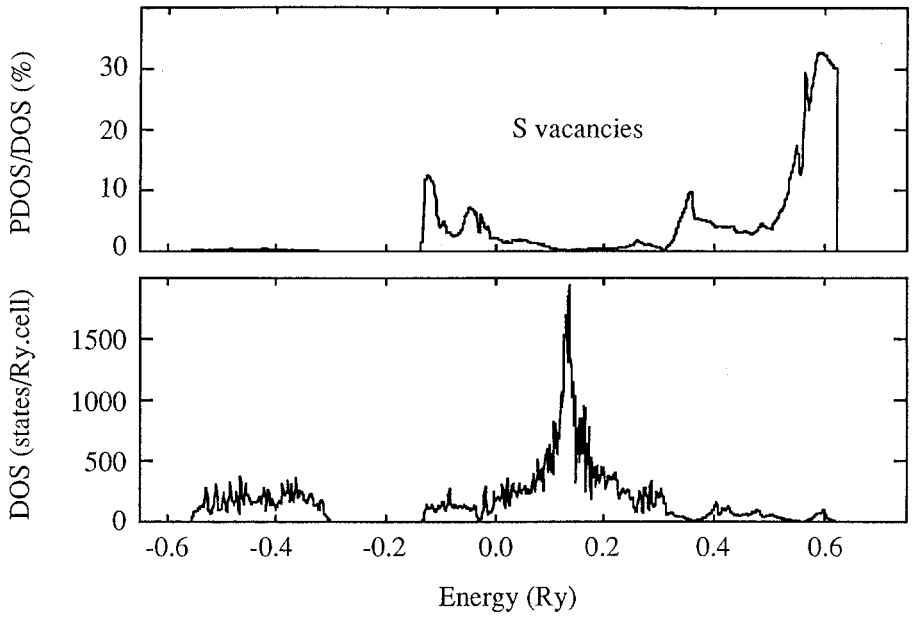

FIG. 6. DOS of lacunar $La_{12}S_{15}$ and relative projected density of states per atom, PDOS/DOS, of the sulfur vacancies of $La_{12}S_{15}$ in the cb region.

pair. Besides, if the distance between the neighbor metal atoms is sufficiently small, a new metal–metal hybridization across the vacancy site emerges which also lowers the energy of the local state. As a result, the local state drops down from the continuum of the conductivity band. Moreover, an antibonding counterpart of this localized state appears above the top of the *d* band.

Figure 6 is a good demonstration of the foregoing speculations. The S vacancy states are, as expected, high in energy around 0.5–0.6 Ry. An S vacancy "sharp" impurity peak is clearly visible at the bottom of cb at ca. -0.12 Ry, while at ca. 0.35 Ry its antibonding counterpart is found. An analysis of the La_3S_4 and $La_{12}S_{15}$ energy curves (not shown in this report) reveals a flattening of the bands near the bottom of

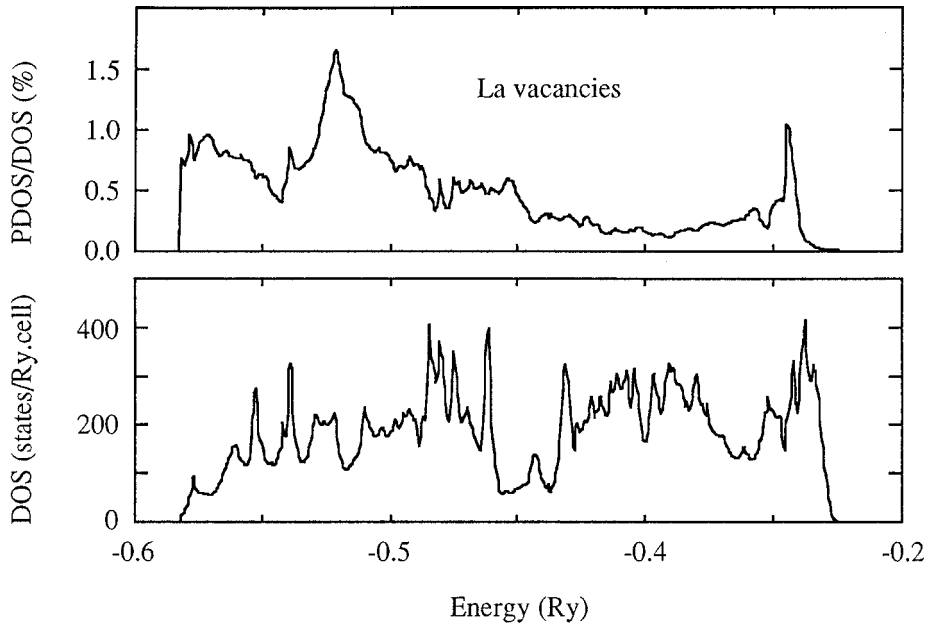

FIG. 7. DOS of lacunar La_5S_7 and relative projected density of states per atom, PDOS/DOS, of the lanthanum vacancies of La_5S_7 in the vb region.

the conductivity zone in the Γ-H and H-N directions, which corresponds to the state localization.

Obviously, an analogous discussion can be carried out for the vacancies in the metal sublattice. When a metal atom is removed, a bonding state near the bottom of the valence band disappears. Instead, a local state emerges at higher energy inside the valence band. In addition, with the loss of screening interactions, this local state can gain a certain amount of sulfur–sulfur antibonding character, which further raises its energy. A bonding counterpart should appear at lower energy. In our calculation the metal vacancy states are found in the 0.3–0.6 Ry region, but they are not important for the optical properties. As predicted, local La vacancy impurity states appear at the top of vb at ca. 0.28 Ry, as can be seen in Fig. 7, with the bonding counterpart being found at the bottom of vb. The comparison between the band structure of La_3S_4 and La_2S_3 also reveals that the occurrence of the peak at the top of vb is related to a flattening of the bands along the Γ-P-N direction, that is to a localization of the states. Similar results were obtained from the Ce derivative.

Finally, the band structure calculations show that localized states near the bottom of cb and near the top of vb can be present arising from vacancies in the nonmetal sublattice and in the metal sublattice, respectively.

IV. CONCLUDING REMARKS

The results obtained with the EHTB methods are qualitatively good. However, *ab initio* TB LMTO-ASA calculations provide a much deeper insight into the electronic structure of the $Ln_{3-x}S_4$ rare earth sulfides, in which the $4f$ orbital participation in the chemical bonding has to be taken into account. This allows a rationalization of a series of properties of the doped and undoped γ-Ln_2S_3 (Ln = La, Ce, Pr, Nd): electrical behavior, color origin and evolution, and occurrence of trap levels revealed by photoconductivity and fluorescence studies.

ACKNOWLEDGMENTS

The research has been made possible by a grant (# 80-02815-00) from Rhône-Poulenc Chimie. VPZ acknowledges also the financial support of the Ministry of Science and Education of Spain for his sabbatical leave in Spain, where a part of this work was done. PG thanks Dr. M. A. Perrin and Dr. E. Wimmer for fruitful remarks and discussion on the first version of this work.

REFERENCES

1. G. Velleret and J.-M. Tourre, "Proceedings of ANTEC93," New Orleans, Society of Plastic Engineering (1993).
2. (a) R. Mauricot, M. Evain, P. Gressier, and R. Brec, *J. Alloys Comp.* **223,** 130 (1995); (b) R. Mauricot, Thesis, University of Nantes, 1995.
3. (a) M.-H. Whangbo and R. Hoffmann, *J. Am. Chem. Soc.* **100,** 6093 (1978); (b) M.-H. Whangbo, R. Hoffmann, and R. B. Woodward, *Proc. R. Soc. London, Ser. A* **366,** 23 (1979).
4. C. Witz and M. L. Theye, private communication.
5. S. Kaciulis, A. Latisenka, and A. Plesanovas, *Surf. Sci.* **251/252,** 330 (1991).
6. (a) P. Hohenberg and W. Kohn, *Phys. Rev. B* **136,** 864 (1964); (b) W. Kohn and L. J. Sham, *Phys. Rev. A* **140,** 1133 (1965).
7. (a) O. K. Andersen, *Phys. Rev. B* **12,** 3060 (1975); (b) H. L. Skriver, "The LMTO Method," Springer–Verlag, Berlin, 1984.
8. (a) V. I. Anisimov, J. Zaanen, O. K. Andersen, *Phys. Rev. B* **44,** 943 (1991); (b) V. I. Anisimov, I. V. Solovyev, M. A. Korotin, M. T. Czyzyk, and G. A. Sawatzky, *Phys. Rev. B* **48,** 16929 (1993); (c) V. I. Anisimov, O. Gunnarsson, *Phys. Rev. B* **43,** 7570 (1991).
9. (a) S. Balle, J. Costa-Quintana, and F. Lopez-Aguilar, *Phys. Rev. B: Cond. Matter.* **37,** 6615 (1988); (b) F. Lopez-Aguilar, S. Balle, and J. Costa-Quintana, *Phys. Rev. B: Cond. Matter.* **38,** 163 (1988).
10. O. Jepsen and O. K. Andersen, *Z. Phys. B* **97,** 35 (1995)
11. J. P. Perdew and A. Zunger, *Phys. Rev. B* **23,** 5048 (1981).
12. Z. Szotek, W. M. Temmerman, and H. Winter, *Physica B* **172,** 19 (1991).
13. (a) O. K. Andersen and O. Jepsen, *Phys. Rev. Lett.* **53,** 2571 (1984); O. K. Andersen, O. Jepsen, and D. Glötzel, *in* "Highlights of Condensed Matter Theory" (F. Bassani, F. Fumi, and M. P. Tosi, Eds.), p. 59. North-Holland, New York, 1985; (b) O. K. Andersen, O. Jepsen, and M. Sob, *in* "Electronic Band Structure and its Applications" (M. Yussouf, Ed.), p. 1. Springer–Verlag, Berlin, 1986; (c) W. R. Lambrecht and O. K. Andersen, *Phys. Rev. B* **34,** 2439 (1986).
14. P. E. Blöchl, O. Jepsen, and O. K. Andersen, *Phys. Rev. B* **49,** 16223 (1994).
15. "Gmelin Handbook of Inorganic Chemistry, C7, Sulfides," p. 85–106. Springer–Verlag, Berlin, 1983.
16. (a) M. Cutler, R. L. Fitzpatrick, and J. F. Leavy, *J. Phys. Chem. Solids* **24,** 319 (1963); (b) M. Cutler and J. F. Leavy, *Phys. Rev. A* **133,** 1153 (1964).
17. (a) V. P. Zhuze and A. I. Shelykh, *Sov. Phys. Semicond.* **23,** 245 (1989); (b) S. A. Kutolin, R. N. Samoilova, L. F. Belova, M. N. Korotkovitch, O. M. Kotenko, and G. M. Komarova, *J. Struct. Chem.* [*USSR*] **13,** 226 (1972).
18. G. Babonas, R. Dagis, and G. Pukinskas, *Phys. Status Solidi B* **153,** 741 (1989).
19. V. P. Zhuze, A. A. Kamarzin, M. G. Karin, K. K. Sidorin, and A. I. Shelykh, *Sov. Phys. Solid State* **21,** 1968 (1979).
20. A. N. Georgiobani, M. V. Glushkov, A. A. Kamarzin, E. S. Logozinskaya, Yu. N. Malovitskii, Zh. A. Pukhlii, V. V. Sokolov, I. M. Tiginyanu, and I. A. Shcherbakov, *Sov. J. Quantum Electron.* **12,** 972 (1982).
21. R. Mauricot, J. Bullot, J. Wery, M. Evain, *Mater. Res. Bull.* **31,** 263 (1996).
22. T. M. Batirov, K. A. Verkhovskaya, A. A. Kamarzin, Yu. N. Malovitskii, V. I. Lisoivan, and V. M. Fridkin, *Sov. Phys. Solid State* **24,** 746 (1982).
23. R. Mauricot, J. Dexpert-Ghys, M. Evain, *J. Lum.* **69,** 41 (1996).
24. G. Hormandiger, J. Redinger, P. Weinberger, G. Hobiger, and P. Herzig, *Solid State Commun.* **68,** 467 (1988).
25. (a) P. Marksteiner, P. Weinberger, A. Neckel, R. Zeller, P. H. Dederichs, *Phys. Rev. B* **33,** 6709 (1986); (b) P. Marksteiner, P. Weinberger, A. Neckel, R. Zeller, and P. H. Dederichs, *J. Phys. F* **16,** 1495 (1986).